

Article

Microscopic Diffusion Characteristics of Linear Alkylbenzene Sulfonates on the Surface of Anthracite: The Influence of Different Attachment Sites of Benzene Ring in the Backbone

Xuanlai Chen ¹, Guochao Yan ^{1,*}, Xianglin Yang ², Guang Xu ^{3,*} and Shuai Wei ⁴¹ School of Mining Engineering, Taiyuan University of Technology, Taiyuan 030024, China; cxlcxl111@126.com² Hunan Provincial Key Laboratory of Fine Ceramics and Powder Materials, School of Materials and Environmental Engineering, Hunan University of Humanities, Science and Technology, Loudi 417000, China; Xianglin.Yang@curtin.edu.au³ Department of Mining Engineering, Missouri University of Science and Technology, Rolla, MO 65409, USA⁴ China Coal Technology & Engineering Group, Taiyuan Research Institute Co., Ltd., Taiyuan 030006, China; 15834123430@163.com

* Correspondence: yanguochao@tyut.edu.cn (G.Y.); guang.xu@mst.edu (G.X.)

Abstract: In order to explore the effect of the attachment site of the benzene ring in the backbone of the surfactant on its diffusion characteristics on the surface of anthracite, the molecular dynamics simulation method was used, and the four isomers (m-C16, m = 2,4,6,8; m represents the attachment site of the benzene ring in the backbone) of sodium hexadecyl benzene sulfonate (SHS) were selected. Binary models of surfactant/anthracite, surfactant/graphene modified by oxygen-containing functional groups, and a ternary model of water/surfactant/anthracite were constructed. By analyzing a series of properties such as interaction energy, contact surface area, relative concentration distribution, radial distribution function, hydrophobic tail chain order parameter, etc., it is concluded that the adsorption strength of 4-C16 on the surface of anthracite is the highest; the reason is that 4-C16 has the highest degree of aggregation near the oxygen-containing functional groups on the surface of anthracite. Further investigations find that 4-C16 can be densely covered on the ketone group, and the longer branch chain of 4-C16 has the highest degree of order in the Z-axis direction.

Keywords: diffusion characteristics; molecular dynamics; isomers; anthracite; benzene ring

Citation: Chen, X.; Yan, G.; Yang, X.; Xu, G.; Wei, S. Microscopic Diffusion Characteristics of Linear Alkylbenzene Sulfonates on the Surface of Anthracite: The Influence of Different Attachment Sites of Benzene Ring in the Backbone. *Minerals* **2021**, *11*, 1045. <https://doi.org/10.3390/min11101045>

Academic Editor: Hegoi Manzano

Received: 26 August 2021

Accepted: 24 September 2021

Published: 27 September 2021

Publisher's Note: MDPI stays neutral with regard to jurisdictional claims in published maps and institutional affiliations.



Copyright: © 2021 by the authors. Licensee MDPI, Basel, Switzerland. This article is an open access article distributed under the terms and conditions of the Creative Commons Attribution (CC BY) license (<https://creativecommons.org/licenses/by/4.0/>).

1. Introduction

Surfactants are amphiphilic compounds and are widely used in a variety of industry applications [1–4] (e.g., in the cosmetics, food, polymer paint, and coal industries). In terms of applicability, cost-effectiveness, and overall consumption level, linear alkyl benzene sulfonate (LAS) is one of the most important surfactant series [5–7]. LAS consists of a sulfonate group and a linear alkyl chain connected to the 1, 4 positions of the benzene ring (Figure 1). Commercial LAS surfactants are usually complex mixtures of homologues [8,9], i.e., different positions on the alkyl chain where the benzene ring is attached, and structural isomers. Heterogeneity means that LAS exhibits different performances, such as different surface tension and solubility, and it is widely used in detergents, cosmetics, and mineral extraction [10–12]. However, this heterogeneity also increases the difficulty of elaborating the detailed mechanisms and functions of LAS members. So far, many studies have been conducted on LAS mixtures [13–15], and relatively few studies on isomers.

In the coal industry, surfactants have been widely used in coal flotation and coal dust suppression [16–20]. Research on coal flotation and coal dust suppression relies on the basic theory of coal wettability [16,21–23]. Existing experimental research has proved that diffusion characteristics of surfactants on a coal surface are an important factor affecting the wettability of coal [23–28]. However, the experimental method cannot explain the structure, dynamics, and energy characteristics of the molecular adsorption

process on the coal surface. Molecular dynamics (MD) simulation can explain the above characteristics [29–32].

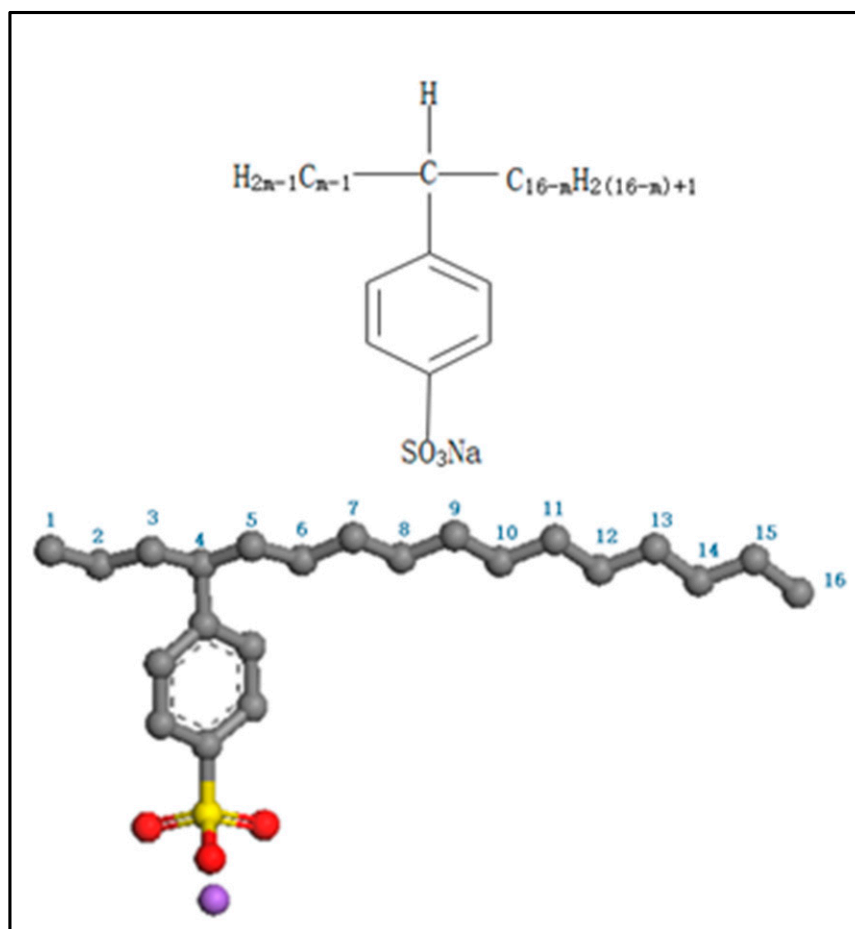


Figure 1. The isomers of SHS ($m = 2,4,6,8$), and the example shown is 4-C16.

Through computer simulation, the microstructure and macroscopic properties of the surfactant system can be linked. In particular, MD simulation has proven to be a very useful tool for studying the structure and dynamics of surfactants at the molecular level. At present, a large number of MD simulation studies have been conducted on the diffusion of other surfactants on the surface of coal [29–31], but there are few studies on the diffusion characteristics of LAS on the surface of coal [20,24].

In the previous research work, we used molecular dynamics simulation to explore the microscopic reasons for the different diffusion characteristics of SDS and SDBS on the surface of anthracite [32] and concluded that the presence of benzene rings in the surfactant has an important impact on the diffusion characteristics. Liu et al. [24] compared a large number of surfactants with different structures through experiments and concluded that the presence of the benzene ring in the surfactant has a significant impact on the hydrophilicity of coal. In order to further explore the microscopic mechanism of the influence of the benzene ring on diffusion characteristics, in this study, we applied the four isomers of SHS of the LAS family. We chose the four isomers of the LAS family because they exist in nature and the only difference they have is that the benzene ring has a different connection position on the carbon chain. The above two reasons lead us to believe that these four isomers are the ideal materials we need, which can realize the subject of “the influence of different attachment sites of benzene ring in the backbone” well that we want to study. MD simulations were performed. As far as we know, this is the first attempt to systematically

study and compare the diffusion characteristics of LAS family members on the surface of anthracite through MD simulation.

Through the MD simulation of the surfactant/anthracite binary system, the interaction energy and the contact surface area of the four isomers were compared, and the macroscopic conclusion that 4-C16 had the highest adsorption strength on the coal surface was obtained. We constructed a surfactant/oxygen-containing functional group modified graphite layer binary system and analyzed the relative concentration distribution to explain the microscopic reason for the highest adsorption strength of 4-C16 from the perspective of functional groups. In order to study the compactness of the layered structure formed by surfactant diffusion, a water layer was added to construct a water/surfactant/anthracite ternary system. The radial distribution function, coordination number, and hydrophobic tail chain sequence parameters were analyzed, and the results show that the 4-C16 layer is the densest, and the effect of “isolating” water molecules is the best. We then tried to explain its microscopic reasons. This research explored the microscopic reasons for the difference in the degree of aggregation caused by the different connection sites of the benzene ring in the backbone. What is more, this research fills the gap in the study of the adsorption characteristics of LAS on the surface of anthracite, enriches and develops the basic theory of coal wettability, and also provides technical ideas for the design of new surfactants.

2. Materials and Methods

2.1. Materials

This study selects Jincheng anthracite coal (from No. 3 coal seam underground in Zhaozhuang Coal Mine, Jincheng). Table 1 shows the results of proximate and ultimate analyses of this coal [33]. The analysis of the other characteristics of Jincheng anthracite can be seen in Figures S1–S4 and Tables S1 and S2.

Table 1. Proximate and ultimate analyses of Jincheng anthracite.

Proximate Analysis				Ultimate Analysis				
M_{ad}	A_d	V_{daf}	FC_d	C	H	O	N	S
0.66	23.05	12.86	67.05	91.51	3.89	2.10	1.71	0.79

M_{ad} : Moisture content on an air-dried basis. A_d : Ash content on dry basis. V_{daf} : Volatile content (in ash-free form), FC_d : Fixed carbon content.

The surfactants used in this study are the four isomers of SHS represented by m-C16 (Figure 1), and the benzene ring is connected to the m th carbon in the hexadecane backbone. The reason for choosing them is that the length of the backbone of these four isomers is the same, and the benzene ring is connected at different positions of the backbone, which is convenient for studying the influence of the benzene ring on the diffusion characteristics. The benzene ring divides the backbone into two parts, the shorter one is defined as a short-chain branch, and the longer one is defined as a long-chain branch. As shown in Figure 1, in 4-C16, carbons 1-4 constitute a short-chain branch, and carbons 4-16 constitute a long-chain branch.

2.2. Computational Details

As shown in Figure 2a, the molecular structure of Jincheng anthracite proposed by our team was used to construct an anthracite model [33]. It can be seen that there are two oxygen-containing functional groups, namely ketone and hydroxyl. Through the Amorphous Cell module of Materials Studio 6.0, 40 optimized coal molecules (ratio 1:1) were randomly packed in a cubic simulation cell $35 \times 35 \times 35 \text{ \AA}^3$ (X Y Z) to obtain a low-density three-dimensional structure model. Then 300 ps molecular dynamics simulations were performed to adjust the crystal cell structure continuously using the NVT ensemble (the constant-temperature, constant-volume ensemble) and NPT ensemble (the constant-temperature, constant-pressure ensemble), so that the density of coal molecular structure

reached a balance [30], as shown in Figure 3. The final 3D coal structure model is shown in Figure 2b.

After MD simulation, the final density of the anthracite model is $1.24 \text{ g}\cdot\text{cm}^{-3}$. This density was obtained by dividing the molecular weight of the coal by the volume of the unit cell, but there are many pores of different sizes on the surface of the coal (the blue part in Figure 2b). The existence of pores causes this density to not be the true density of anthracite.

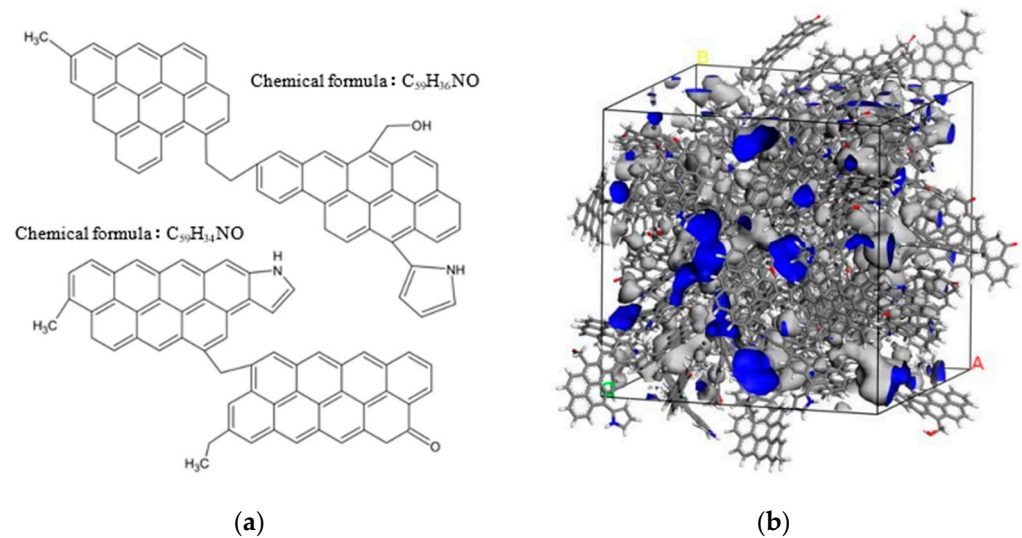


Figure 2. (a) Molecular structure of Jincheng Anthracite; (b) 3D structure model of Jincheng Anthracite (the blue part indicates the pores).

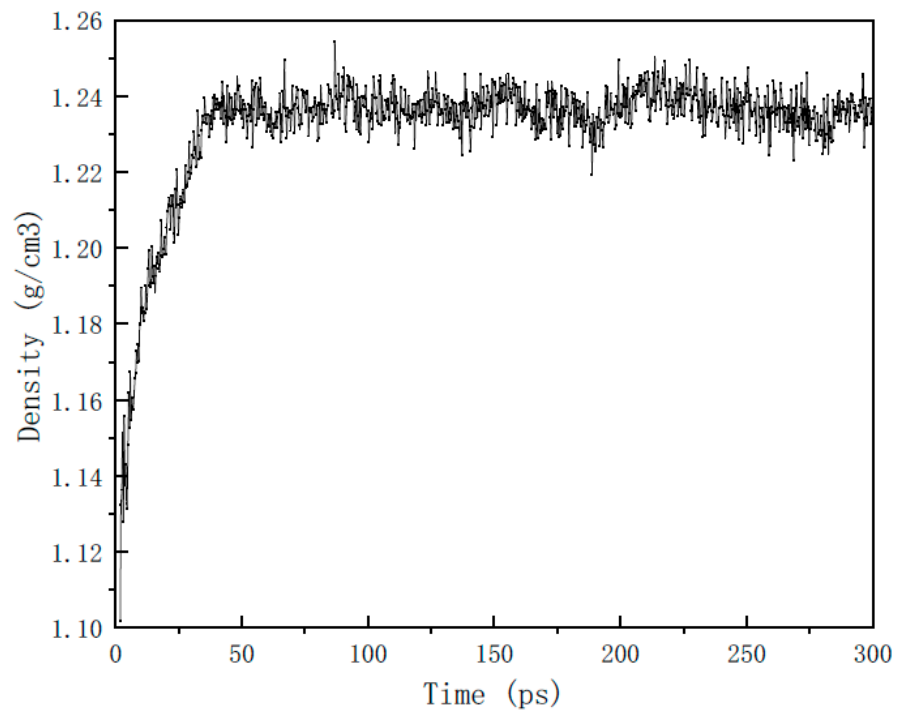


Figure 3. Change of calculated density with time.

In fact, in the measurement of coal density, in order to obtain the true density of coal, helium is usually used as a detection gas to remove holes in the coal. The simulated helium density of Jincheng anthracite was calculated using Atom Volumes & Surfaces

in Material Studios software, helium was used as the detection gas, and the dynamic radius was 0.129 nm [34]. In our previous study [35], the density of Jincheng anthracite measured by experiments was $1.43 \text{ g}\cdot\text{cm}^{-3}$. The true density of the anthracite model calculated by the above method is $1.38 \text{ g}\cdot\text{cm}^{-3}$, which is close to the measured density of $1.43 \text{ g}\cdot\text{cm}^{-3}$. Considering that the measured density of coal may also contain other impurities or minerals (gangue, fly ash, etc.) [36], the theoretical model only considers the structure of the coal itself. It is believed that the constructed coal model is reasonable and can be used to further study the adsorption behavior of surfactants. We constructed surfactant/anthracite and water/surfactant/anthracite models. The surfactant layer is a rectangular unit cell containing 10 surfactant molecules, and the unit cell size is the same as the anthracite surface model. Water slabs were composed of 1000 water molecules. MD simulations were performed in the Forcite module of Materials Studio. The polymer consistent force field (PCFF) was used to describe the intermolecular interaction in all simulations. In order to fully eliminate the adverse interaction between atoms, before MD simulation, A smart algorithm was used to minimize the energy of the anthracite surface model, the surfactant cell, and the water slab. Subsequently, MD simulations were performed in the NVT ensemble. The temperature was set to 298 K, and the 1000 ps simulation was performed at a time step of 1 fs, so that the systems reached a fully balanced state. In all MD simulations, the Ewald method was used to calculate the electrostatic interactions with a precision of 0.001 kcal/mol, and the tom-based option was used to calculate the van der Waals interactions with a cut-off of 1.25 nm. The above simulations were all carried out in a unit cell with periodic boundary conditions. At the top of every model, a 6 nm vacuum layer was built to eliminate the mirror effect. The bottom two-thirds of the anthracite surface model were constrained, and the top one-third was free. In a large number of atomic systems, this method will greatly save calculation time. According to the research of Zhang et al. [31], this restrictive method has basically no effect on the calculation results.

The surfactant/oxygen-containing functional group-modified graphite layer system model was constructed with 4 surfactant molecules combined with a hydroxyl-modified graphite layer and a ketone-modified graphite layer, respectively. We first built the graphite layer, then we modified the surface of the graphite layer with ketone groups and hydroxyl groups, respectively, to obtain the modified graphite layer model, and then we assembled the 4 surfactant molecules with the modified graphite layer model together using the build layer tool. After geometric optimization minimized the energy of the system, a 1000 ps MD simulation was performed, and the parameter settings were the same as the above parameters.

3. Results and Discussion

3.1. Surfactant/Anthracite Adsorption System

The initial and final adsorption configurations of surfactants on the surface of anthracite coal are shown in Figure 4. When the surfactant layer was placed on the surface of the coal model, the surfactant/anthracite system became thermodynamically unstable. Driven by van der Waals interaction and electrostatic potential, the surfactants diffused to the surface of the coal model and were finally adsorbed [29]. After a 1000 ps MD simulation, a new thermodynamic equilibrium state was reached.

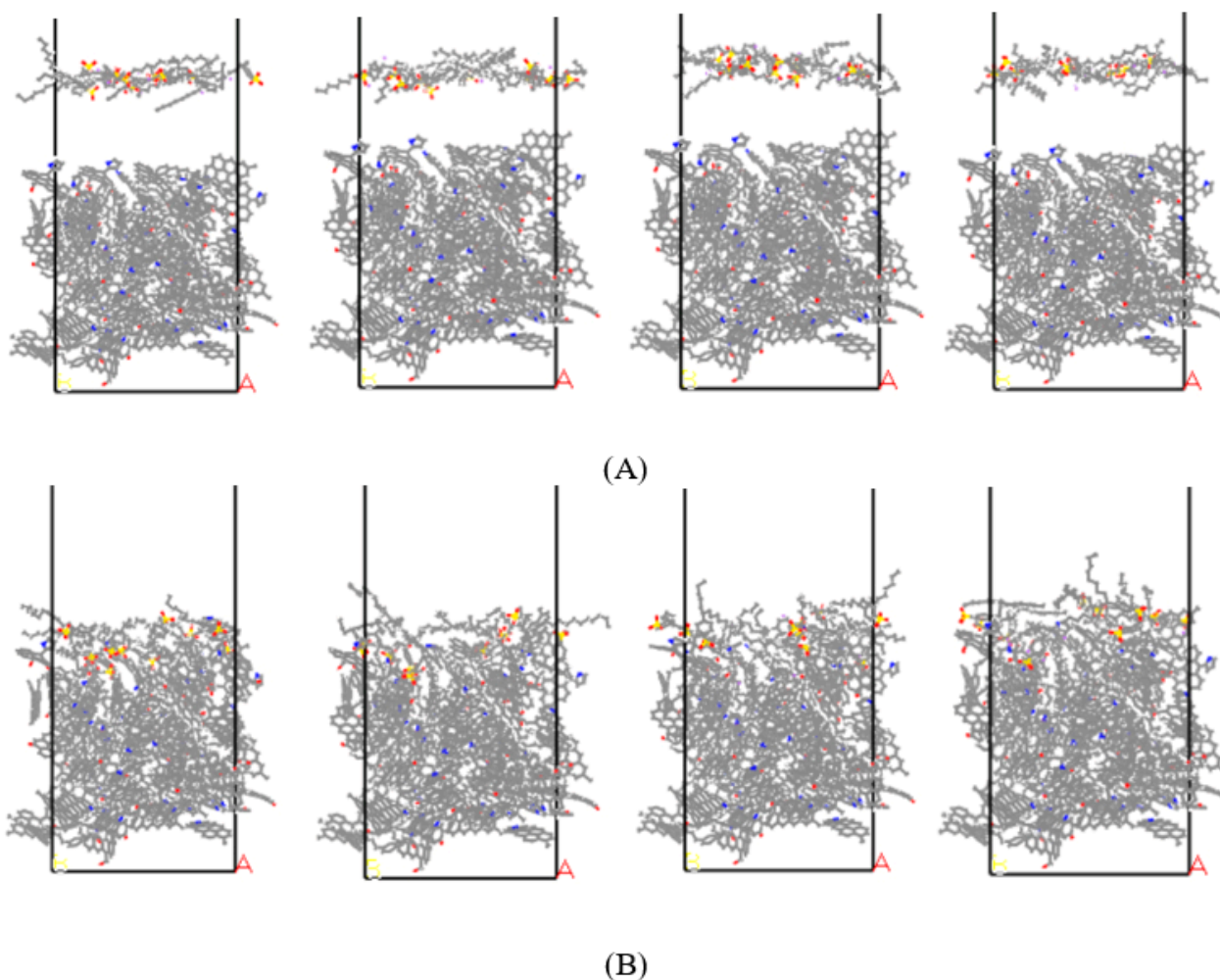


Figure 4. From left to right is the m-C16/anthracite system ($m = 2,4,6,8$). (A) Initial configuration; (B) final configuration.

3.1.1. Interaction Energy

The interaction energy of the surfactant and the anthracite after adsorption can be used to evaluate the adsorption strength. The more negative the interaction energy, the more energy is released, the more stable the structure after adsorption, and the higher the adsorption strength [37,38]. It should be pointed out that the interaction energy here only represents the strength of the interaction between the surfactant and the anthracite surface. It is not equal to the thermodynamic adsorption energy. The magnitude of the interaction energy also depends on the force field parameters used in the simulation [19,39]. It can be calculated by the following formulas:

$$EV = EV_{total} - EV_{coal} - EV_{surf} \quad (1)$$

$$EL = EL_{total} - EL_{coal} - EL_{surf} \quad (2)$$

$$E = EV + EL \quad (3)$$

where EV represents the van der Waals interaction energy, EL represents the electrostatic interaction energy, E represents the total interaction energy, E_{total} is the total energy of surfactant and anthracite, E_{coal} is the anthracite energy, and E_{surf} is the surfactant energy. The results are shown in Table 2.

Table 2. Interaction energy between the surfactant and anthracite.

Model	$EV/(\text{kcal}\cdot\text{mol}^{-1})$	$EL/(\text{kcal}\cdot\text{mol}^{-1})$	$E/(\text{kcal}\cdot\text{mol}^{-1})$
2-C16/Anthracite	−277.92	−2.23	−280.15
4-C16/Anthracite	−293.77	−6.54	−300.31
6-C16/Anthracite	−273.07	−3.01	−276.08
8-C16/Anthracite	−257.94	−3.29	−261.23

The interaction energy is negative, indicating that the entropy of the reaction increases and the reaction proceeds spontaneously. Comparing the total interaction energy data in Table 2, the total interaction energy of the 4-C16/anthracite system was the lowest, indicating that the 4-C16 adsorption process emitted the most energy, the adsorption strength was the highest, and the formed adsorption system was the most stable. This is due to the difference in the molecular structure of surfactants. The four isomers of SHS have the same polar head group and different attachment positions of the benzene ring in the backbone, resulting in different branch chain lengths. When $m = 2$, the short-chain branch carbon chain is shorter and appears rigid, and there is a certain steric hindrance effect. When $m = 4$, the influence on the aggregation behavior of the surfactant is the greatest. Under the combined action of steric hindrance and the hydrophobic interaction, the degree of aggregation is the densest, and the adsorption strength is higher than other systems. As the value of m is further increased, the flexibility of the short-chain branch increases, and the hydrophobic interaction force with the long-chain branch increases, which reduces the intermolecular interaction, resulting in a decrease in the adsorption strength [24,40]. To gain deeper insight into the adsorption mechanism of the collector, the components of interaction energy were analyzed [41,42]. The van der Waals interaction energy is far greater than the electrostatic interaction energy, and it plays a leading role in the adsorption of anthracite and surfactants. This is because the electrostatic interaction is a long-range interaction, with a range of several nanometers [43]. Although the simulation model satisfies the distance condition, because anthracite is a type of high-rank coal, the total number of oxygen-containing functional groups on the surface is small, and the electronegativity is small, so the number of atoms with different charges in the molecules of anthracite and anionic surfactants is small, which leads to a very small charge difference between anthracite particles and surfactants [44]. Therefore, the electrostatic attraction between the oppositely charged parts is weak, so that the electrostatic interaction only accounts for a very small part of the total interaction energy.

3.1.2. Contact Surface Area

In addition to the interaction energy, the contact surface area (CSA) is introduced to evaluate the adsorption strength, and a larger CSA indicates a stronger adsorption strength. The CSA can be calculated using Equation (4):

$$CSA = \left(SASA_{coal} + SASA_{collector} - SASA_{complex} \right) / 2 \quad (4)$$

where $SASA_{coal}$, $SASA_{collector}$, and $SASA_{complex}$ are the solvent-accessible surface areas (SASA) of the anthracite model, collector, and anthracite/collector complex, respectively.

In this study, we used a probe with a radius of 1.4 Å to calculate the solvent-accessible surface area [22,31]. The calculation result is shown in Figure 5.

The calculation results show that the CSA between 4-C16 and anthracite is the largest. This is due to the fact that as the sulfonate group moves to the middle of the backbone, the short-chain branch becomes longer, resulting in a size change of the hydrophobic part of the surfactant molecule. According to the literature [3,45–47], when the size of the hydrophobic group and the hydrophilic group is similar, the surfactant molecule almost covers the entire interface, and the CSA is the largest at this time. It shows that the size of the hydrophobic part composed of the short-chain branch composed of 4 carbon atoms and the long-chain branch composed of 12 carbon atoms in 4-C16 is similar to the size of the

hydrophilic group of benzenesulfonic acid, which leads to the largest CSA with anthracite. The results of contact surface area match well with the interaction energy results.

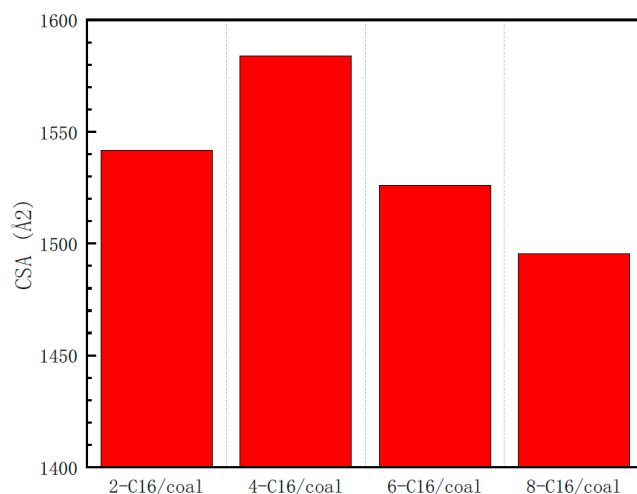


Figure 5. The contact surface areas of different models.

3.2. Graphite Layer System

Studies have shown that oxygen-containing functional groups on the surface of coal affect the diffusion of surfactants [22,48,49]. To explore the distribution of surfactants on oxygen-containing groups of anthracite, a graphene model grafting different oxygen functional groups (carbonyl and ketone) was constructed, as shown in Figure 6. Due to the high degree of coalification of anthracite, its molecular structure is composed of aromatic layers, similar to graphite. The graphite layer system can simulate the surface of anthracite coal after modifying the graphite flakes with oxygen-containing functional groups [33,50,51].

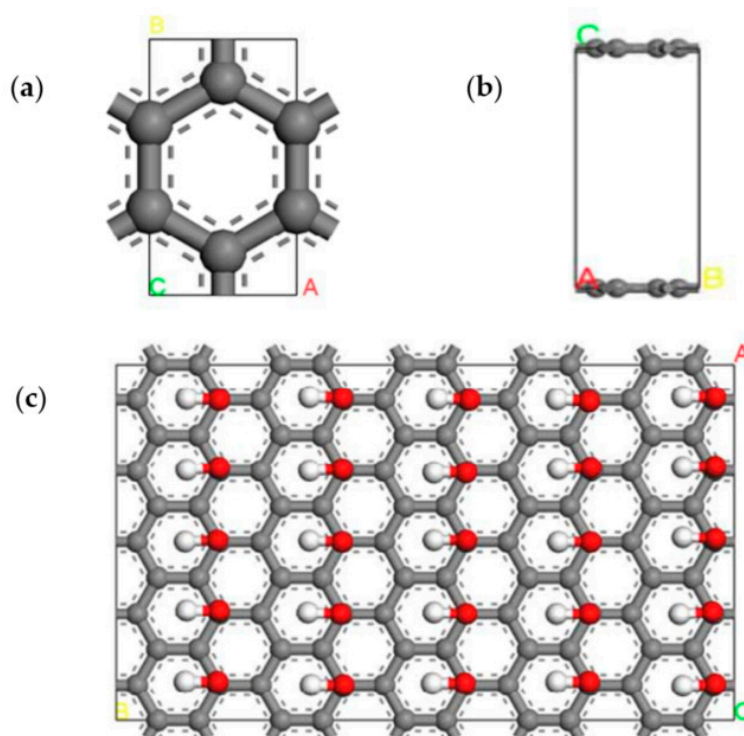


Figure 6. (a) The top view; (b) the side view of graphite, and (c) a hydroxyl-modified graphite layer.

3.2.1. Adsorption Configuration

Four surfactant molecules were placed on the surface of the graphite layer system to build a surfactant/graphene modified by oxygen-containing functional groups system. The system reached equilibrium after a 1000 ps MD simulation, and the final equilibrium configurations are shown in Figure 7. It can be seen intuitively that 4-C16 has the highest degree of aggregation near the hydroxyl group and forms the densest layered structure.

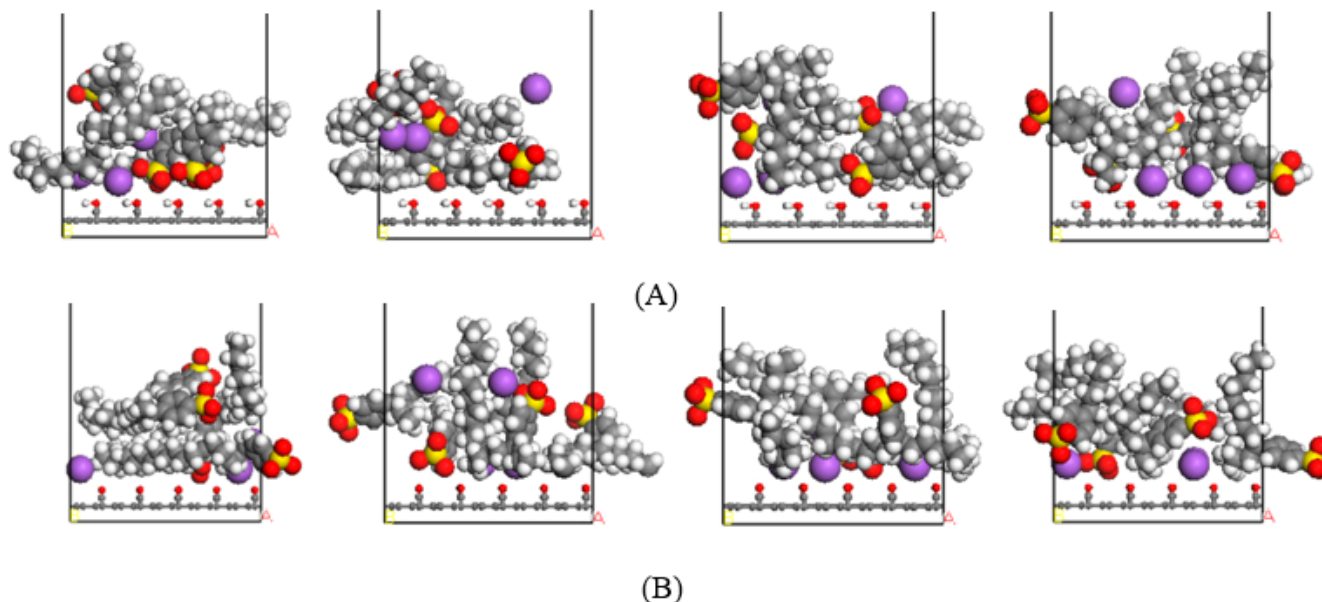


Figure 7. From left to right is the m-C16/anthracite system ($m = 2,4,6,8$). (A) The final adsorption configuration after equilibrium on the hydroxyl-modified graphite layer; (B) the final adsorption configuration after equilibrium on the ketone-modified graphite layer (the purple spheres represent sodium ions).

3.2.2. Relative Concentration Distribution

The relative concentration distribution along the Z axis can obtain the distribution of each component along the Z axis. Analyzing the distribution range of the surfactant along the Z axis and the relative concentration peak height in different systems can explain and compare the aggregation degree of the surfactant [19,42,52]. The last 500 ps data of the simulation were selected for analysis, and the relative concentration distribution of different surfactants along the Z axis is shown in Figure 8.

It can be found that regardless of whether on the hydroxyl group or the ketone group, the relative concentration distribution of these four isomers has two peaks. This is related to the adsorption method. The anionic surfactant is dominated by a van der Waals force on the coal surface. There are two adsorption methods: the adsorption of the head group toward the coal surface and the adsorption away from the coal surface [26]. The appearance of two peaks also proves that the modified graphite layer model can simulate the coal surface well.

On the hydroxyl group, the first peak appeared near 0.7 nm, and the peak value of the first peak of 4-C16 is about 6.48, which is much higher than the other three surfactants, indicating that 4-C16 has the highest degree of aggregation near the hydroxyl group. It can be found that the starting point of the relative concentration distribution curve of the four surfactants along the Z axis is the same, but the end point of 4-C16 reaches the X axis first, indicating that the 4-C16 distribution width is the narrowest and the most compact near the hydroxyl group. The relative concentration peak of 4-C16 is the highest and the distribution width is the narrowest, indicating that 4-C16 has the densest degree of aggregation and the highest adsorption strength near the hydroxyl group.

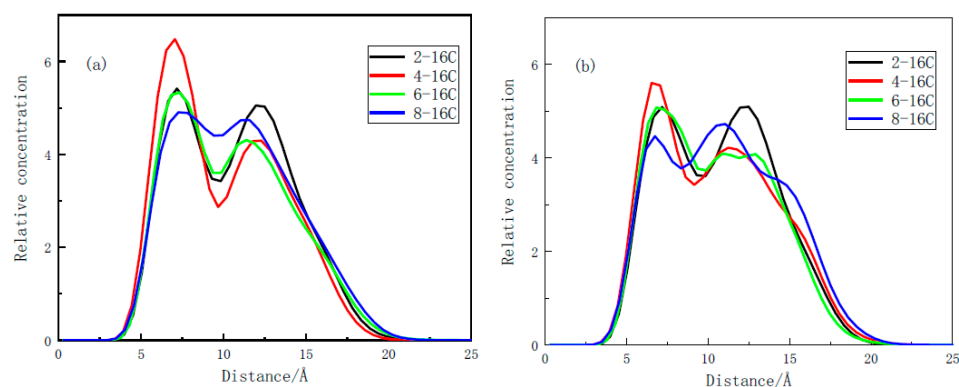


Figure 8. The relative concentration distribution of the four surfactants on (a) the hydroxyl group; (b) the ketone group along the Z axis.

On the ketone group, the first peak of 4-C16 is about 5.6, which is the highest among the four isomers, indicating that it has the highest degree of aggregation near the ketone group. It can also be found that the heights of the two peaks of 2-C16 are similar regardless of whether it is near the hydroxyl group or the ketone group, and the second peak is higher than the other three surfactants. It is speculated that this is because the steric hindrance effect of 2-C16 in the rigid short-chain branch at $m = 2$ causes it to be more inclined to stay away from the coal surface [3,19,40]. Furthermore, according to existing research [9], the shorter the alkane chain, the lower the viscosity, the weaker the intermolecular force is, and the easier it is to produce a translation, rotation, and deformation when subjected to other forces. The short-chain branch of 2-C16 makes it more inclined to stay away from the coal surface. It is found that the heights of the peaks near the hydroxyl and ketone groups of 8-C16 are similar, but the distance between the two peaks is the shortest among the four surfactants. It is speculated that this is due to the difference between the short-chain and long-chain branches of 8-C16 by only one carbon. At this time, the length of the short-chain branch and the long-chain branch are similar. In addition, the hydrophobic interaction between the pliable short-chain branch and the long-chain branch is enhanced, resulting in a smaller difference between 8-C16 in the two adsorption methods.

It can be concluded that the reason for the highest adsorption strength of 4-C16 on the surface of anthracite is that it has the densest degree of aggregation and the highest adsorption strength near the oxygen-containing functional groups on the surface of anthracite. The conclusion is consistent with the following radial distribution function and coordination number analysis.

3.3. Water/Surfactant/Anthracite System

In order to further explore the diffusion characteristics of the four isomers of SHS in the aqueous solution and the compactness of the layered structure, a slab composed of 1000 water molecules was added to the modified coal, then a water/surfactant/anthracite system model was built. After adding the water slab, the system became thermodynamically unstable. After a 1000 ps MD simulation, the system tended to be stable again. The equilibrium configuration of the water/surfactant/anthracite system is shown in Figure 9.

The addition of surfactants is equivalent to adding a “protective layer” on the surface of anthracite or a “separation layer” of water molecules [22]. The “protection” or “isolation” effect makes it difficult for water molecules to penetrate the anthracite. The “isolation” ability of water molecules is used to evaluate the compactness of the layered structure, and further analyze the microscopic reasons for the different compactness through the radial distribution function (RDF), coordination number, and hydrophobic tail chain order parameters.

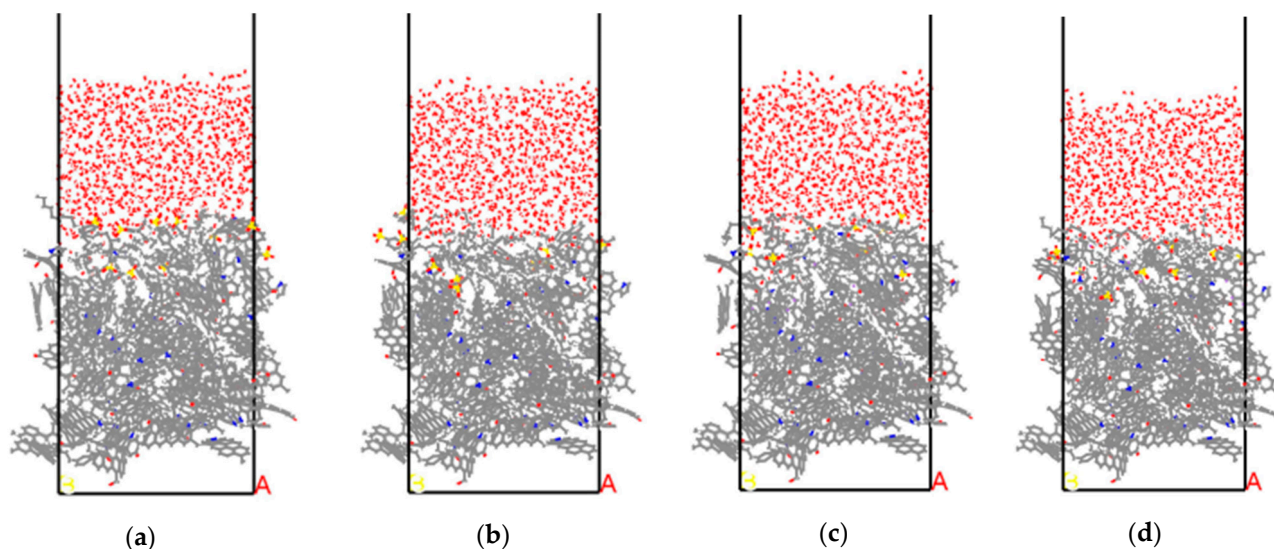


Figure 9. Equilibrium configuration of the water/surfactant/anthracite system after MD simulation (a) 2-C16; (b) 4-C16; (c) 6-C16; (d) 8-C16.

3.3.1. Radial Distribution Function

The adsorption of water molecules on the coal surface first occurs on the hydrophilic functional groups, because they have a strong affinity with water molecules. The RDF between atoms can determine the degree of aggregation of water molecules on the oxygen-containing functional groups of anthracite. Through the calculation of the coordination number, the isolation effect of water molecules after adding the surfactant can be quantified. The RDF is calculated using Equation (5). The height of the first peak formed by the RDF between atoms indicates the degree of order between the water molecules and the functional groups on the coal surface, and the high and sharp peaks indicate the strong order and strong interaction between atoms [53–57].

$$g(r) = \frac{1}{4\pi\rho_B r^2} \cdot \frac{dN}{dr} \quad (5)$$

where ρ_B represents the density of particle B; r is the distance between B and A; and dN is the average number of particle B in the range r to $r + dr$ from A as the reference particle.

The RDF between O_C (oxygen atoms on the surface of coal) and O_W (oxygen atoms in water molecules) is calculated and plotted in Figure 10. The four curves obtained are quite different, which indicates that the attachment of the benzene ring at different positions has different effects on the hydrophobicity of the coal surface.

The water/8-C16/anthracite system has the highest peak with a peak value of about 0.26, the water/6-C16/anthracite system has a peak value of about 0.2, and the water/2-C16/anthracite system has a peak value of about 0.17. No obvious peaks are observed in the RDF of the water/4-C16/anthracite system, indicating that the interaction strength between O_C atoms and O_W atoms in this system was relatively weak, with only few water molecules gathering around the oxygen atoms on the coal surface. It shows that 4-C16 has the best “isolation” effect on water, the layered structure formed is the densest, and the adsorption strength is the highest. The “isolation” ability of water is ranked as 4-C16 > 6-C16 > 8-C16 > 2-C16, which is consistent with the above CSA analysis results.

In order to further explore the microscopic reasons for the strongest water “isolation” of 4-C16, the RDF between O_H (Oxygen atoms in hydroxyl groups on coal surface), O_K (Oxygen atom in ketone group on coal surface), and O_W in the four systems was calculated. The results are shown in Figure 11.

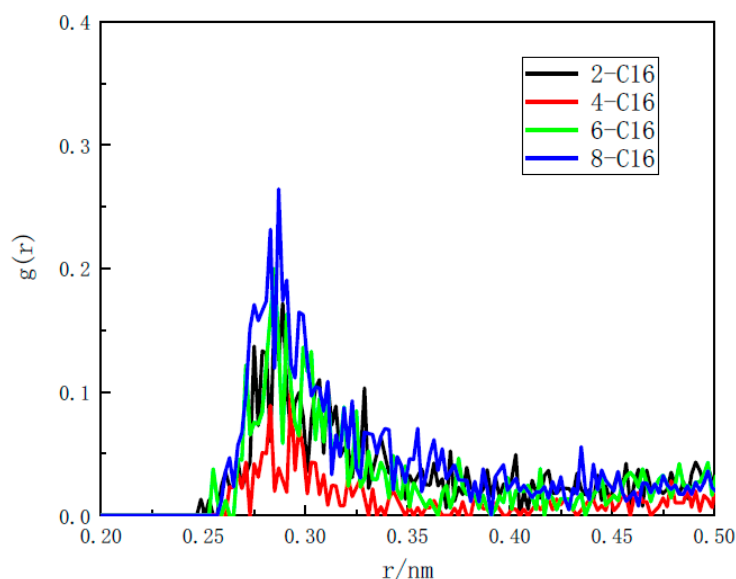


Figure 10. The RDF between O_C and O_W .

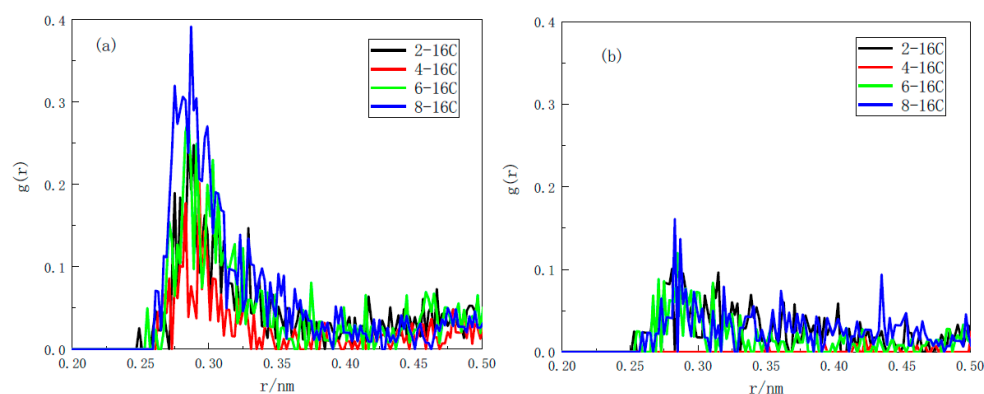


Figure 11. The RDF of (a) O_H and O_W ; (b) O_K and O_W .

Analyzing Figure 11a, it can be seen that the water/8-C16/anthracite system has the highest peak, with a peak value of about 0.39, the water/6-C16/anthracite system has a peak balance of about 0.28, and the water/4-C16/anthracite system has a peak value of about 0.17, while the peak value of the water/2-C16/anthracite system is about 0.26. The minimum 4-C16 peak indicates that the layered structure formed near the hydroxyl group is the densest, making it the strongest in its ability to “isolate” water.

In analyzing Figure 11b, it can be found that the RDF of the water/4-C16/anthracite system is almost zero, and the RDF peaks of the other three systems are not much different, indicating that 4-C16 can completely “isolate” the water near the ketone group, densely covering the surface of the ketone group. The other three isomers have a similar ability to “separate” water near the ketone group.

In general, the coordination number (the number of B atoms around the A atom) is an effective parameter for evaluating the strength of the interaction between atoms [29]. The higher the coordination number, the stronger the interaction between atoms. We calculated the coordination number of O_w around O_H and O_K . The coordination number is calculated by the following formula:

$$dN = \frac{g(r) \cdot N \cdot 4\pi r^2 dr}{V} \quad (6)$$

where N is the total number of B atoms and V is the periodic model volume. The calculation results are shown in Figure 12.

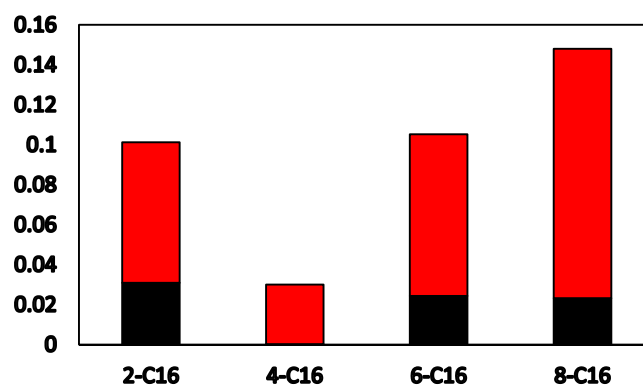


Figure 12. Coordination numbers of different functional groups (red indicates the coordination number of O_H and O_w, black is the coordination number of O_K and O_w).

It can be seen that the ketone coordination number of 4-C16 is almost zero, and the ketone coordination number of the other three isomers is almost the same. The order of the coordination numbers around the hydroxyl group is 4-C16 < 2-C16 < 6-C16 < 8-C16. The above analysis is consistent with the RDF analysis.

Based on the analysis of the RDF and the coordination number, it is concluded that 4-C16 has the densest layered structure in aqueous solution and the strongest ability to “isolate” water. The reason is that (a) 4-C16 can densely cover the ketone group on the surface of anthracite, completely “isolating” water from contact with the ketone group; the other three isomers have similar water isolation ability near the ketone group; (b) 4-C16 has the best effect of “isolating” water near the hydroxyl group, far stronger than the other three isomers. This is consistent with the relative concentration distribution analysis results.

3.3.2. Surfactant Molecular Orientation

The molecular orientation of surfactants is another important property, which explains the different cohesive phases formed by amphiphilic molecules [40,58]. We defined two vectors, θ_b (the benzene vector) and θ_t (the tail vector) and calculated the inclination angle of these two vectors with respect to the interface normal (Z axis). θ_b is defined as the vector from the sulfur atom to the carbon atom in the backbone connected to the benzene ring. This vector passes through the benzene plane. θ_t is defined as the vector from the carbon atom in the backbone connected to the benzene ring to the carbon atom at the end of the longer branch [9]. We calculated the benzene vector and tail vector of each surfactant in the system and took the arithmetic average. The average θ_b and average θ_t are shown in Figure 13.

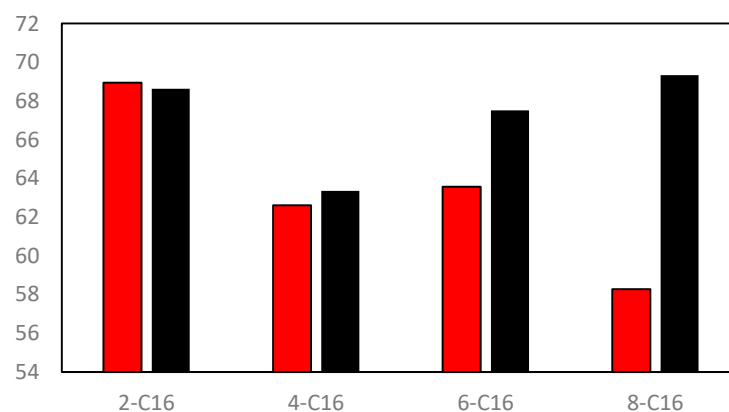


Figure 13. Average benzene vector and average tail vector (red is θ_b and black is θ_t).

It can be seen that with the increase in m , the gap between the benzene vector and the tail vector of the same m value becomes larger and larger, indicating that the head group and the longer hydrophobic tail chain increasingly tend not to be in a straight line. This is because as the attachment site of the benzene ring moves to the middle of the carbon chain, the short-chain branch becomes longer and the long-chain branch becomes shorter, and the hydrophobic interaction between the short-chain branch and the long-chain branch increases, resulting in an increase in mutual repulsion between them, resulting in the long-chain branch offsetting the benzene vector.

It can also be found that the change trend of the hydrophobic tail chain is similar to the change trend of the adsorption strength, indicating that the angle of the hydrophobic tail chain is dominant in the adsorption strength. The long hydrophobic tail chain of 4-C16 has the smallest angle with the Z axis, which is about 63° . It causes the surfactants to be closer together and forms a denser layered structure and higher adsorption strength. It can also be seen that the benzene vector of 8-C16 is abnormally small, about 58° . It is speculated that this is because the short-chain and long-chain branches are similar in length, the hydrophobic effect is the strongest, and the long-chain and short-chain branches repel each other, resulting in the largest included angle. At this time, the steric hindrance effect of the tail chain on the hydrophilic group is the smallest, so the hydrophilic head group is freer to face the water phase, resulting in the abnormal minimum of the benzene vector.

To further analyze the microscopic reasons for the influence of the orientation of the longer tail chain on the adsorption strength, we calculated the hydrophobic tail chain order parameter (S_{CD}). It is used to express the order of the hydrophobic tail chain [9,58–60]. The calculation method is shown in formula 7.

$$S_{CD} = \frac{1}{2} \langle 3 \cos^2 \theta_t - 1 \rangle \quad (7)$$

where θ_t is the angle between the tail vector and the Z axis.

The order parameter can vary from $-1/2$ to 1. When the value of S_{CD} is 1, the hydrophobic tail chains are arranged along the vertical direction of the interface. When the value of S_{CD} is $-1/2$, the hydrophobic tail chains are aligned parallel to the interface [60]. The calculation results are shown in Figure 14. The S_{CD} value of 4-C16 is the largest, indicating that it has the highest degree of order in the Z-axis direction. Combined with the above tail vector analysis, the angle between the long branch of 4-C16 and the Z-axis is the smallest, which causes the molecules to be closer and interact better with the surface energy of anthracite, meaning the layered structure formed by 4-C16 is denser and has higher adsorption strength.

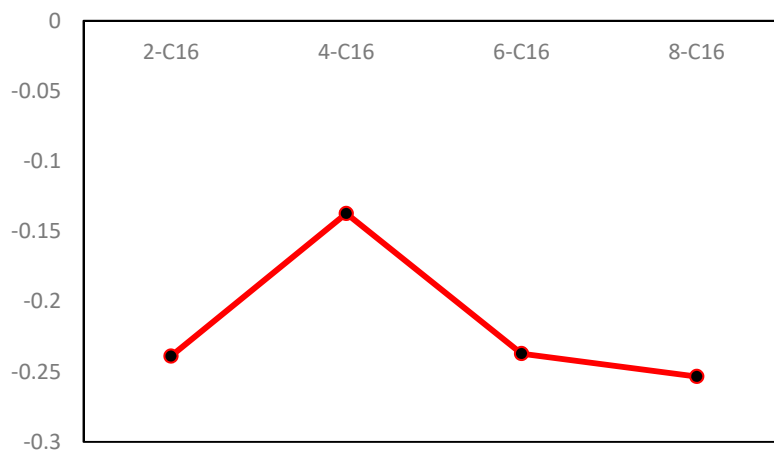


Figure 14. Hydrophobic tail chain order parameter.

4. Conclusions

The MD simulation method was used to study the diffusion characteristics of the four isomers of SHS on the surface of anthracite, and the influence of the different attachment sites of the benzene ring in the backbone on the adsorption strength was discussed. Major findings are as follow:

- (1) The benzene ring has different attachment sites in the backbone and different adsorption strengths. By analyzing the interaction energy of the surfactant–anthracite system and the CSA, it is found that the total interaction energy of the 4-C16/anthracite system is the lowest, while the contact surface area between 4-C16 and anthracite is the largest. It shows that 4-C16 has the highest adsorption strength on the surface of anthracite. The difference in adsorption strength is due to the different structure of the surfactant.
- (2) Through the analysis of the adsorption configuration and relative concentration distribution of the graphite layer system, it is found that the reason for the highest adsorption strength of 4-C16 on the surface of anthracite is that it has the highest adsorption strength near the oxygen-containing functional groups on the surface of anthracite.
- (3) Through the RDF and coordination number analysis of the water/surfactant/anthracite system, it is found that 4-C16 has the highest adsorption strength in the solution and the strongest ability to “isolate” water molecules. The reason is that (a) 4-C16 can densely cover the ketone groups on the surface of anthracite, completely “isolating” water from contact with the ketone groups; (b) 4-C16 has the best effect of “isolating” water near the hydroxyl group. Through surfactant orientation analysis, it is found that the angle between the long-chain branch of 4-C16 and the Z axis is the smallest, and the degree of order in the Z axis is the highest. This is the reason why the layered structure formed by 4-C16 is denser.
- (4) The study of alkyl sulfonate isomers on the surface of anthracite can help in better understanding the influence of the surfactant structure on the adsorption strength. The research results have important theoretical and practical significance for the development of new surfactants and the enrichment and development of the basic theory of coal wettability.

Supplementary Materials: The following are available online at <https://www.mdpi.com/article/10.3390/min11101045/s1>, Figure S1. ¹³C-NMR spectra of a JC anthracite coal sample; Figure S2. Diagram of an image on a lattice image of Jincheng anthracite coal; Figure S3. FTIR spectrum of JC anthracite coal sample; Figure S4. Curve-fitted spectrum in the 700–900, 1000–1800, and 2800–3000 cm^{−1} zone of JC anthracite coal sample; Table S1. Structural assignment frequency obtained from lattice fringe data; Table S2. XPS C (1s), N (1s) and S (2p) data of JC anthracite coal sample.

Author Contributions: Conceptualization, X.C. and S.W.; methodology, X.C. and X.Y.; software, X.C. and G.X.; validation, G.Y. and X.Y.; formal analysis, X.C.; investigation, X.C.; resources, X.C.; data curation, X.C.; writing—original draft preparation, X.C.; writing—review and editing, G.X.; supervision, G.Y.; funding acquisition, G.Y. All authors have read and agreed to the published version of the manuscript.

Funding: This research was funded by the National Natural Science Foundation of China (Grant No. 51974195).

Data Availability Statement: The raw/processed data required to reproduce these findings cannot be shared at this time as the data also form part of an ongoing study.

Conflicts of Interest: The authors declare no conflict of interest.

References

1. Zhang, R.; Sun, C.; Kou, J.; Zhao, H.; Wei, D.; Xing, Y. Enhancing the leaching of chalcopyrite using *Acidithiobacillus ferrooxidans* under the induction of surfactant triton X-100. *Minerals* **2018**, *9*, 11. [\[CrossRef\]](#)
2. Huang, G.; Xu, J.; Geng, P.; Li, J. Carrier flotation of low-rank coal with polystyrene. *Minerals* **2020**, *10*, 452. [\[CrossRef\]](#)
3. Liu, Z.-Y.; Wang, C.; Zhou, H.; Zhang, L.; Zhao, S. Characterizing the impact of surfactant structure on interfacial tension: A molecular dynamics study. *J. Mol. Model.* **2017**, *23*, 112. [\[CrossRef\]](#)
4. Chen, C.-L.; Liao, Y.-F.; Lu, F.; Zheng, Y.-S.; Peng, Y.-Y.; Ding, C.-W.; Tong, Q.-X. Facile synthesis, surface activity, wettability and ultrahigh foaming properties of novel nonionic Gemini fluorocarbon surfactants. *J. Mol. Liq.* **2020**, *302*, 112469. [\[CrossRef\]](#)
5. Askari, A.; Vahabzadeh, F.; Mardanpour, M.M. Quantitative determination of linear alkylbenzene sulfonate (LAS) concentration and simultaneous power generation in a microbial fuel cell-based biosensor. *J. Clean. Prod.* **2021**, *294*, 126349. [\[CrossRef\]](#)
6. Zhao, X.; Gong, L.; Liao, G.; Luan, H.; Chen, Q.; Liu, D.; Feng, Y. Micellar solubilization of petroleum fractions by heavy alkylbenzene sulfonate surfactant. *J. Mol. Liq.* **2021**, *329*, 115519. [\[CrossRef\]](#)
7. Franco-Belussi, L.; Jones-Costa, M.; Salla, R.F.; de Souza, B.F.S.; Pinto-Vidal, F.A.; de Oliveira, C.R.; Silva-Zacarin, E.C.M.; Abdalla, F.C.; Duarte, I.C.S.; De Oliveira, C. Hepatotoxicity of the anionic surfactant linear alkylbenzene sulphonate (LAS) in bullfrog tadpoles. *Chemosphere* **2021**, *266*, 129014. [\[CrossRef\]](#)
8. Chai, L.; Yang, L.; Zhang, Y.; Zhou, Y.; Wang, F.; Wu, Z. Antagonism or synergism? Responses of *Hydrocharis dubia* (Bl.) Backer to linear alkylbenzene sulfonate, naphthalene and their joint exposure. *Ecotoxicol. Environ. Saf.* **2020**, *200*, 110747. [\[CrossRef\]](#)
9. He, X.; Guvench, O.; MacKerell, A.D., Jr.; Klein, M.L. Atomistic simulation study of linear alkylbenzene sulfonates at the water/air interface. *J. Phys. Chem. B* **2010**, *114*, 9787–9794. [\[CrossRef\]](#)
10. Smith, G.A.; Huggett, A.; Jones, C.; Ortego, G. Surface activity and performance properties of gemini salts of linear alkylbenzene sulfonate in aqueous solution. *J. Surfactants Deterg.* **2021**, *24*, 563–574. [\[CrossRef\]](#)
11. Lee, T.; Park, U.; Puligundla, P.; Mok, C. Corona discharge plasma-based degradation of simulated residual linear alkylbenzene sulfonate and dodecyl benzene sulfonate surfactants. *Int. J. Environ. Sci. Technol.* **2019**, *17*, 1171–1178. [\[CrossRef\]](#)
12. Kishimoto, N.; Hamamoto, S. Removal of linear alkylbenzene sulfonate (LAS) by a cetyltrimethylammonium bromide (CTAB)-aided coagulation-filtration process. *Environ. Technol.* **2020**, *42*, 1–9. [\[CrossRef\]](#)
13. Wang, X.P.; Liu, X.C.; Huo, Y.Q.; Niu, J.P. Properties of binary mixture of cetyl biphenyl ether disulfonate and linear alkylbenzene sulfonate. *Tenside Surfactants Deterg.* **2020**, *57*, 259–264. [\[CrossRef\]](#)
14. Koohsaryan, E.; Anbia, M.; Sepehrian, M.; Maghsoodlu, M. Facile hydrothermal synthesis of hierarchical sodium P zeolite as a nonphosphate detergent builder. *J. Surfactants Deterg.* **2021**, *24*, 85–97. [\[CrossRef\]](#)
15. Gang, H.; Bian, P.; He, X.; He, X.; Bao, X.; Mu, B.; Li, Y.; Yang, S. Mixing of surfactin, an anionic biosurfactant, with alkylbenzene sulfonate, a chemically synthesized anionic surfactant, at the n-decane /water interface. *J. Surfactants Deterg.* **2021**, *24*, 445–457. [\[CrossRef\]](#)
16. Liu, Z.; Zhou, G.; Li, S.; Wang, C.; Liu, R.; Jiang, W. Molecular dynamics simulation and experimental characterization of anionic surfactant: Influence on wettability of low-rank coal. *Fuel* **2020**, *279*, 118323. [\[CrossRef\]](#)
17. Han, W.; Zhou, G.; Xing, M.; Yang, Y.; Zhang, X.; Miao, Y.; Wang, Y. Experimental investigation on physicochemical characteristics of coal treated with synthetic sodium salicylate-imidazole ionic liquids. *J. Mol. Liq.* **2021**, *327*, 114822. [\[CrossRef\]](#)
18. Li, L.; He, M.; Li, Z.; Ma, C.; Yu, H.; You, X. Wettability effect of ethoxylated nonyl phenol with different ethylene oxide chain length on Shendong long-flame coal surface. *Mater. Today Commun.* **2021**, *26*, 101697. [\[CrossRef\]](#)
19. Meng, J.; Yin, F.; Li, S.; Zhong, R.; Sheng, Z.; Nie, B. Effect of different concentrations of surfactant on the wettability of coal by molecular dynamics simulation. *Int. J. Min. Sci. Technol.* **2019**, *29*, 577–584. [\[CrossRef\]](#)
20. Lyu, S.; Chen, X.; Shah, S.; Wu, X. Experimental study of influence of natural surfactant soybean phospholipid on wettability of high-rank coal. *Fuel* **2019**, *239*, 1–12. [\[CrossRef\]](#)
21. Yuan, M.; Nie, W.; Zhou, W.; Yan, J.; Bao, Q.; Guo, C.; Tong, P.; Zhang, H.; Guo, L. Determining the effect of the non-ionic surfactant AEO9 on lignite adsorption and wetting via molecular dynamics (MD) simulation and experiment comparisons. *Fuel* **2020**, *278*, 118339. [\[CrossRef\]](#)
22. Li, B.; Liu, S.; Fan, M.; Zhang, L. The effect of ethylene oxide groups in dodecyl ethoxyl ethers on low rank coal flotation: An experimental study and simulation. *Powder Technol.* **2019**, *344*, 684–692. [\[CrossRef\]](#)
23. Yao, Q.; Xu, C.; Zhang, Y.; Zhou, G.; Zhang, S.; Wang, D. Micromechanism of coal dust wettability and its effect on the selection and development of dust suppressants. *Process. Saf. Environ. Prot.* **2017**, *111*, 726–732. [\[CrossRef\]](#)
24. Liu, X.; Liu, S.; Cheng, Y.; Xu, G. Decrease in hydrophilicity and moisture re-adsorption of lignite: Effects of surfactant structure. *Fuel* **2020**, *273*, 117812. [\[CrossRef\]](#)
25. Ni, G.H.; Qian, S.; Meng, X.; Hui, W.; Xu, Y.H.; Cheng, W.M.; Gang, W. Effect of NaCl-SDS compound solution on the wettability and functional groups of coal. *Fuel* **2019**, *257*, 116077.
26. Chang, Z.; Chen, X.; Peng, Y. The interaction between diesel and surfactant triton X-100 and their adsorption on coal surfaces with different degrees of oxidation. *Powder Technol.* **2019**, *342*, 840–847. [\[CrossRef\]](#)
27. Dey, S. Enhancement in hydrophobicity of low rank coal by surfactants—A critical overview. *Fuel Process. Technol.* **2012**, *94*, 151–158. [\[CrossRef\]](#)
28. Zhou, P.; Hou, J.; Yan, Y.; Wang, J. The effect of surfactant adsorption on surface wettability and flow resistance in slit nanopore: A molecular dynamics study. *J. Colloid Interface Sci.* **2018**, *513*, 379–388. [\[CrossRef\]](#)

29. Zhang, L.; Li, B.; Xia, Y.; Liu, S. Wettability modification of wender lignite by adsorption of dodecyl poly ethoxylated surfactants with different degree of ethoxylation: A molecular dynamics simulation study. *J. Mol. Graph. Model.* **2017**, *76*, 106–117. [CrossRef]
30. Zhang, H.; Xi, P.; Zhuo, Q.; Liu, W. Construction of molecular model and adsorption of collectors on bulianta coal. *Molecules* **2020**, *25*, 4030. [CrossRef]
31. Zhang, Z.; Wang, C.; Yan, K. Adsorption of collectors on model surface of wiser bituminous coal: A molecular dynamics simulation study. *Miner. Eng.* **2015**, *79*, 31–39. [CrossRef]
32. Chen, X.L.; Yan, G.C.; Yang, X.L.; Feng, Z.Z.; Wei, S. Molecular Dynamics Simulation of the Effect of SDS/SDBS on the Wettability of Anthracite. *Coal Science and Technology*. Available online: <https://kns.cnki.net/kcms/detail/11.2402.TD.20210623.1502.004.html> (accessed on 23 June 2021).
33. Wei, S.; Yan, G.C.; Zhang, Z.Q.; Liu, M.S.; Zhang, Y.F. Molecular structure analysis of jincheng anthracite coal. *J. China Coal Soc.* **2018**, *43*, 555–562.
34. Zheng, M.; Li, X.; Liu, J.; Guo, L. Initial chemical reaction simulation of coal pyrolysis via. ReaxFF molecular dynamics. *Energy Fuels* **2013**, *27*, 2942–2951. [CrossRef]
35. Yan, G.; Ren, G.; Bai, L.; Feng, J.; Zhang, Z. Molecular model construction and evaluation of jincheng anthracite. *ACS Omega* **2020**, *5*, 10663–10670. [CrossRef] [PubMed]
36. Li, Q.; Liu, D.M.; Cai, Y.D.; Zhao, B.; Qiu, Y.K.; Zhou, Y.F. Scale-span pore structure heterogeneity of high volatile bituminous coal and anthracite by FIB-SEM and X-ray mu-CT. *J. Nat. Gas. Sci. Eng.* **2020**, *81*, 103443. [CrossRef]
37. Li, J.; Han, Y.; Qu, G.; Cheng, J.; Xue, C.; Gao, X.; Sun, T.; Ding, W. Molecular dynamics simulation of the aggregation behavior of N-Dodecyl-N,N-Dimethyl-3-Ammonio-1-Propanesulfonate/sodium dodecyl benzene sulfonate surfactant mixed system at oil/water interface. *Colloids Surf. A Physicochem. Eng. Asp.* **2017**, *531*, 73–80. [CrossRef]
38. Anvari, M.H.; Liu, Q.; Xu, Z.; Choi, P. Molecular dynamics study of hydrophilic sphalerite (110) surface as modified by normal and branched butylthiols. *Langmuir* **2018**, *34*, 3363–3373. [CrossRef]
39. Rai, B.; Sathish, P.; Tanwar, J.; Pradip; Moon, K.; Fuerstenau, D. A molecular dynamics study of the interaction of oleate and dodecylammonium chloride surfactants with complex aluminosilicate minerals. *J. Colloid Interface Sci.* **2011**, *362*, 510–516. [CrossRef]
40. Chen, Y.J.; Zhou, H.T.; Ge, J.J.; Xu, G.Y. Aggregation behavior of double-chained anionic surfactant 1-C_m-C-9-SO₃Na at air/liquid interface: Molecular dynamics simulation. *Acta Phys. Chim. Sin.* **2017**, *33*, 1214–1222. [CrossRef]
41. Kubelka, J.; Bai, S.; Piri, M. Effects of surfactant charge and molecular structure on wettability alteration of calcite: Insights from molecular dynamics simulations. *J. Phys. Chem. B* **2021**, *125*, 1293–1305. [CrossRef]
42. Xia, Y.; Yang, Z.; Zhang, R.; Xing, Y.; Gui, X. Enhancement of the surface hydrophobicity of low-rank coal by adsorbing DTAB: An experimental and molecular dynamics simulation study. *Fuel* **2019**, *239*, 145–152. [CrossRef]
43. Liu, Q.; Yuan, S.; Yan, H.; Zhao, X. Mechanism of oil detachment from a silica surface in aqueous surfactant solutions: Molecular dynamics simulations. *J. Phys. Chem. B* **2012**, *116*, 2867–2875. [CrossRef] [PubMed]
44. He, X.; Liu, X.; Song, D.; Nie, B. Effect of microstructure on electrical property of coal surface. *Appl. Surf. Sci.* **2019**, *483*, 713–720. [CrossRef]
45. Li, Z.-Q.; Wang, L.; Cao, X.-L.; Song, X.-W.; Zhang, L.; Zhao, S.; Yu, J.-Y. Influence of alkyl chain length and position on microenvironmental properties of alkylbenzenesulfonates micelles. *J. Dispers. Sci. Technol.* **2009**, *30*, 65–67. [CrossRef]
46. Cui, X.-H.; Wang, L.; Cao, X.-L.; Zhao, F.-L.; Luo, L.; Zhang, L.; Zhao, S.; Yu, J.-Y. Effect of additional alkyl substituents on the adsorption properties of sodium branched-alkylbenzenesulfonates. *J. Dispers. Sci. Technol.* **2008**, *29*, 1153–1157. [CrossRef]
47. He, X.; Shinoda, W.; DeVane, R.; Anderson, K.L.; Klein, M.L. Paramaterization of a coarse-grained model for linear alkylbenzene sulfonate surfactants and molecular dynamics studies of their self-assembly in aqueous solution. *Chem. Phys. Lett.* **2010**, *487*, 71–76. [CrossRef]
48. Wang, W.; Liang, L.; Peng, Y.; Holuszko, M. Surface chemical heterogeneity of low rank coal characterized by micro-FTIR and its correlation with hydrophobicity. *Minerals* **2021**, *11*, 239. [CrossRef]
49. Liu, X.; Liu, S.; Fan, M.; Zhang, L. Decrease of hydrophilicity of lignite using CTAB: Effects of adsorption differences of surfactant onto mineral composition and functional groups. *Fuel* **2017**, *197*, 474–481. [CrossRef]
50. Zhang, L.; Guo, J.; Hao, M.; Li, B.; Liu, S. Microscopic spreading characteristics of non-polar oil droplet on low rank coal surface: Effects of surfactant pretreatment and oxygen-containing groups. *J. Mol. Liq.* **2021**, *325*, 115232. [CrossRef]
51. Zhang, L.; Sun, X.; Li, B.; Xie, Z.; Guo, J.; Liu, S. Experimental and molecular dynamics simulation study on the enhancement of low rank coal flotation by mixed collector. *Fuel* **2020**, *266*, 117046. [CrossRef]
52. Zhang, R.; Xing, Y.; Xia, Y.; Luo, J.; Tan, J.; Rong, G.; Gui, X. New insight into surface wetting of coal with varying coalification degree: An experimental and molecular dynamics simulation study. *Appl. Surf. Sci.* **2020**, *511*, 145610. [CrossRef]
53. Yan, H.; Guo, X.-L.; Yuan, S.-L.; Liu, C.-B. Molecular dynamics study of the effect of calcium ions on the monolayer of SDC and SDSn surfactants at the vapor/liquid interface. *Langmuir* **2011**, *27*, 5762–5771. [CrossRef] [PubMed]
54. Yang, J.-S.; Yang, C.-L.; Wang, M.-S.; Chen, B.-D.; Ma, X.G. Crystallization of alkane melts induced by carbon nanotubes and graphene nanosheets: A molecular dynamics simulation study. *Phys. Chem. Chem. Phys.* **2011**, *13*, 15476–15482. [CrossRef] [PubMed]
55. Xu, J.; Zhang, Y.; Chen, H.; Wang, P.; Xie, Z.; Yao, Y.; Yan, Y.; Zhang, J. Effect of surfactant headgroups on the oil/water interface: An interfacial tension measurement and simulation study. *J. Mol. Struct.* **2013**, *1052*, 50–56. [CrossRef]

56. Parra, J.G.; Iza, P.; Dominguez, H.; Schott, E.; Zarate, X. Effect of triton X-100 surfactant on the interfacial activity of ionic surfactants SDS, CTAB and SDBS at the air/water interface: A study using molecular dynamic simulations. *Colloids Surf. A Physicochem. Eng. Asp.* **2020**, *603*, 125284. [[CrossRef](#)]
57. Xu, Y.; Liu, Y.-L.; Liu, G.-S. Molecular dynamics simulation of primary ammonium ions with different alkyl chains on the muscovite (001) surface. *Int. J. Miner. Process.* **2015**, *145*, 48–56. [[CrossRef](#)]
58. Takeda, K.; Andoh, Y.; Shinoda, W.; Okazaki, S. Molecular behavior of linear alkylbenzene sulfonate in hydrated crystal, tilted gel, and liquid crystal phases studied by molecular dynamics simulation. *Langmuir* **2019**, *35*, 10877–10884. [[CrossRef](#)]
59. Stanishneva-Konovalova, T.; Sokolova, O. Molecular dynamics simulations of negatively charged DPPC/DPPI lipid bilayers at two levels of resolution. *Comput. Theor. Chem.* **2015**, *1058*, 61–66. [[CrossRef](#)]
60. Vermeer, L.; De Groot, B.L.; Reat, V.; Milon, A.; Czaplicki, J. Acyl chain order parameter profiles in phospholipid bilayers: Computation from molecular dynamics simulations and comparison with ²H NMR experiments. *Eur. Biophys. J.* **2007**, *36*, 919–931. [[CrossRef](#)]